ACADEMIA ROMÂNĂ
*Revue Roumaine de Chimie*
https://web.icf.ro/rrch/

*Rev. Roum. Chim.*,
**2022**, *67*(8–9), 503–510
DOI: 10.33224/rrch.2022.67.8-9.09

# PHOTODEGRADATION OF SUNSET YELLOW BY $TIO_2/SNO_2$ NANOCOMPOSITES FILMS DEPOSITED USING SPRAY PYROLYSIS

Abdelmadjid ABABSA,[a,b*] Akila BENAISSA,[c] Youcef BELLAL,[b] Nail El Houcine BARAMA,[d] Antar BOUHANK,[b] Khaled HAMDI-CHERIF [b] and Noureddine GHERRAF[e]

[a] Laboratory of Process Engineering for the Environment (LIPE), Department of Environmental Engineering, Faculty of Process Engineering, Salah Boubnider University, Constantine 3, Constantine 25000, Algeria
[b]Research Center in Industrial Technologies CRTI, P. O. Box 64, Cheraga 16014, Algeria
[c]Faculty of Process Engineering, Department of Pharmaceutical Engineering, Laboratory of Process Engineering for the Environment (LIPE), Salah Boubnider University, Constantine 3, Constantine 25000, Algeria
[d]L.T.T.S.M. University of Constantine 1, 25017, Constantine, Algeria
[e]Laboratory of Natural Resources and Management of Sensitive Environments, University of Larbi Ben Mhidi, Oum El Bouaghi, Algeria

*Received September 3, 2022*

The main objective of the work in hand is to investigate the degradation of sunset yellow dye under UV light using the $TiO_2$ and $SnO_2$ as photocatalysts. Thin films of $TiO_2$ (T), $SnO_2$ (S) and their nanocomposite (TS) were deposited by spray pyrolysis on glass substrate at 550 °C. According to X-ray diffraction (XRD), all the films had a polycrystalline structure. The S film had traces of SnO and the T film was a mixture of anatase and rutile. The TS film was a combination of anatase, rutile and $SnO_2$. The grain size decreased from 115 nm in S to 21.5 and 18.8 nm in T and TS films respectively. Tensile strain was present in all films. The UV-Vis spectra revealed relatively higher transmittance in TS and T and lesser in S. Using the Tauc plot, the optical gap energy was calculated to be 3.60, 3.17 and 3.71 eV for S, T and TS respectively. The surface morphology examined by SEM showed homogenous grain with different shapes and sizes. The photodegradation of sunset yellow dye after 18 hours was ameliorated in the TS film to reach 90.27% where the S and T films had 19.74 and 29.65 degradation percentage respectively. The photocatalysis kinetics was found to fit a first order chemical reaction.

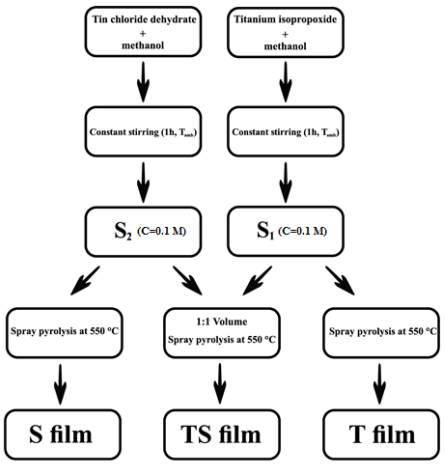


## INTRODUCTION

Dyes are extensively used to color products in a variety of industries, including fabrics, materials, leather, decorations and paints, photographs, cosmetic and pharmaceutical products, biological pigments, and food. AZO dyes currently account for the majority of dye chemistry production volume, and their importance may grow in the future.[1] In fact, approximately 70% of all the dyes used in industry are azo dyes.[2] The harmful effects of AZO dyes on humans and aquatic life, on the other hand, have prompted urgent calls for the treatment of AZO dye-containing effluents in order to get rid of them or convert them into useful and safe products.[3] Actually, these dyes are classified as emerging pollutants because, even at low concentrations, they have complex chemical

* Corresponding author: abdelmadjid.ababsa@gmail.com

structures and mechanisms of action that make proper removal from water and wastewater difficult. These waste waters can have a number of effects on the receiving water bodies, including reduced solar infiltration and changes in photosynthetic activity and biochemical oxygen demand. Furthermore, if these compounds are ingested by humans, they can cause serious health problems due to their high carcinogenic, mutagenic, and teratogenic potential. As a result, these pollutants must be monitored and properly removed from the environment. The Conventional physical, chemical and biological procedures hold limitations and are avowed deficient in the removal of dyes, due to the stability of their chemical structure in adverse conditions.[4]

Sunset yellow is a member of the AZO dyes group and like the rest of the AZO, at low concentrations (order of 1 ppm), in drinking water and lakes can cause significant damage and potential health issues. In order to remove this environmental threat, further researches are being carried out in order to find out how to reduce the risk of damage, using different methods among which photodegradation by means of metal oxides.[5]

Titanium dioxide ($TiO_2$) is a multifunctional material and has attracted great attention because of its exceptional catalytic and semiconductor features. Nowadays, with the onset of nanotechnology, titanium dioxide powder and films have been widely investigated due to its new properties obtained by reducing particle size, including high chemical stability, non-toxicity, high oxidizing power, biocompatibility, high dielectric constant and transmittance and wide band gap energy (3.0–3.2 eV).[6] These properties make $TiO_2$ an excellent material for different applications such as water separation for hydrogen generation,[7] antimicrobial surfaces,[8] solar cells,[9] gas sensors[10] and self-cleaning coatings for urban buildings.[11] In addition, $TiO_2$-based thin films are being used as a photocatalyst in a wide range of environmental remediation techniques especially in studying the degradation of organic pollutants. However, there are many limitations that must be overcome to improve their efficiency and decrease the rapid recombination of photogenerated charge carriers.[12] $TiO_2$ thin films in general crystalize as anatase, rutile, or a mixture of both. The anatase phase being more reactive is frequently used in photocatalytic applications.[13] One important approach to overcome the quick recombination of photogenerated charge carriers is forming $TiO_2$ composites. Many such composite semiconductor systems have been proposed as photocatalysts: $TiO_2$-$SiO_2$,[14] $TiO_2$–ZnO,[15] $TiO_2$–CuO,[16] CdO–$TiO_2$–CuO.[17] In this regard, $SnO_2$ was chosen as the second compound for the preparation of $TiO_2$-$SnO_2$ nanocomposites. Tin oxide ($SnO_2$) is an n-type semiconductor material that shows interesting properties such as a wide band gap ranging from 3.6 to 3.8 eV,[18] high transparency in the visible region, high electrical conductivity, good adhesion to glass, low expenses and good stability in various weather conditions. These properties make tin oxide suitable for many applications, particularly as a window layer in solar cells,[19] heat reflectors in solar cells,[20] light-emitting diodes,[21] gas sensor,[22] transparent electromagnetic shielding materials,[23] lithium-ion batteries,[24] and optical and photochemical devices in liquid crystal displays.[25]

In this paper, $TiO_2$, $SnO_2$ and $TiO_2$-$SnO_2$ nanocomposite thin films have been prepared by spray pyrolysis technique and used to improve the sunset yellow dye photodegradation by the creation of $TiO_2$-$SnO_2$ heterojucntion as an eco-friendly technique. In the meanwhile, structural, morphological, optical properties of all films were investigated.

## RESULTS AND DISCUSSION

### 1. X-ray diffraction

Fig. 1 displays the XRD patterns of the $TiO_2$, $SnO_2$ and their composite.

According to the JCPDS Card No.: 21-1272, 29-1360, 41-1455 and 06-0395 that identifies anatase $TiO_2$, rutile $TiO_2$, tin(IV) oxide ($SnO_2$) and romarchite (SnO) respectively. We could conclude from Fig. 1 that: the T thin film displayed a mixture of rutile and anatase $TiO_2$. The diffraction planes of rutile were assigned at the positions 27.20, 34.34, 64.81 and 78.68°. The anatase planes were assigned at 38.38, 51.98, 54.92, 61.93, 71.19 and 78.68°. Moreover, the S sample had two crystal structures namely $SnO_2$ and SnO. The first phase was identified at 25.86, 38.91, 53.97 and 70.23°. The SnO crystal phase had two peaks and they were identified at 48.22° and 62.39°. Finally, the TS film was mainly composed of anatase and rutile $TiO_2$ at 27.20, 34.27, 78.60 and 38.28, 51.90, 54.81, 61.92, 78.60° respectively. The $SnO_2$ was discerned at 34.27 and 65.86°.

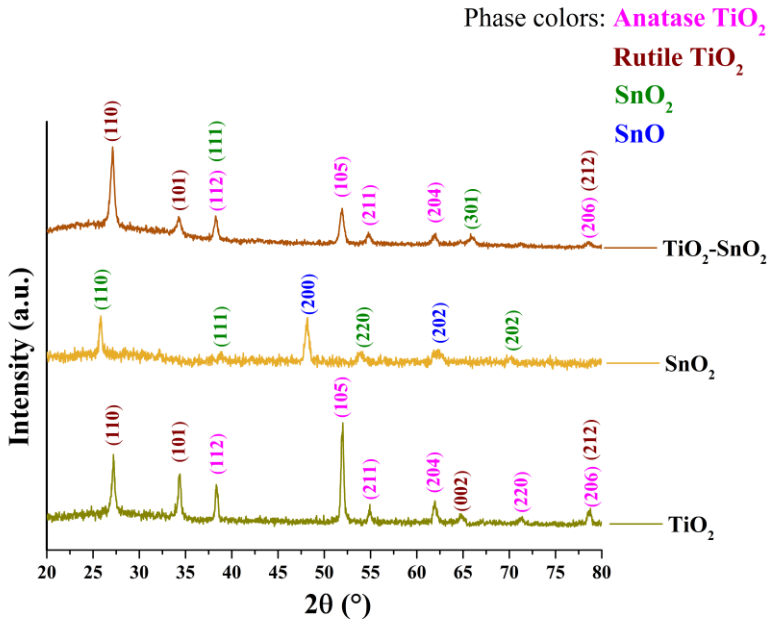


Fig. 1 – X-ray diffraction pattern of the $TiO_2$, $SnO_2$ and their composite elaborated films.

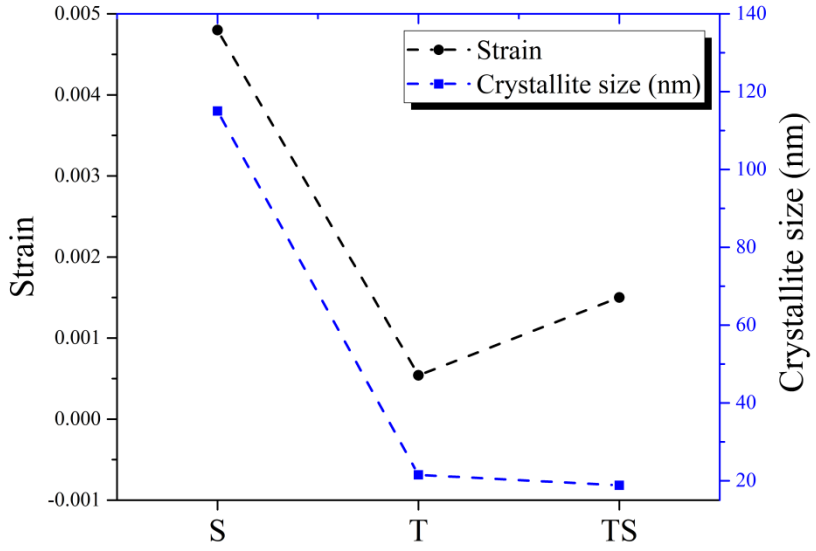


Fig. 2 – Crystallite size and strain of the S, T and TS deposited films.

To calculate the crystallite size and the micro-strain in the films from the Full Width at Half Maximum (FWHM) of the measured peaks, Williamson-Hall method was adopted.[26]

$$FWHM_{total} = FWHM_{crystallite\ size} + FWHM_{strain}$$

The broadening attributed by the crystallite size and strain are given as follows:

$$FWHM_{crystallite\ size} = \frac{K\lambda}{D}\frac{1}{\cos\theta}$$

$$FWHM_{strain} = 4\epsilon\frac{\sin\theta}{\cos\theta}$$

where K=0.9 for Gussian peak fitting, $\lambda$ is the wavelength of X-rays, $D$ is the crystallite size, $\theta$ is the Bragg's angle and $\epsilon$ is the strain. By plotting $FWHM_{total}\cos\theta = a\sin\theta + b$ we could determine the strain from the slop $a = 4\epsilon$ and the crystallite size from the intercept $b = \frac{K\lambda}{D}$.

Fig. 2 depicted the crystallite size and the strain in each film. We could see the remarkable difference in both quantities with respect to S sample ($D = 115\ nm$), as the TS sample registered the lowest crystallite size value of 18.8 nm

and a somewhat medium strain. The decrease in crystallite size in T and TS film relative to the S film can be attributed to the grow competition of different phases present in them, mainly anatase and rutile.[27]

## 2. UV-Vis analysis

The UV-visible spectra, at the wavelength range of 250 to 800 nm for all films, were shown in Fig. 3. The absorption edges around 387 and 344 nm for T and S films respectively shifted with the structure change, *i.e.* the formation of $TiO_2$-$SnO_2$ composite. From the same figure, the TS and T films displayed a relatively high transmittance of around 70% in average in the visible portion of the electromagnetic spectrum (400-800nm); however, the S film's transmittance was around 62%. These values transparency might limit the use of the films in other application such as solar cells. The gap energy was calculated based on the Tauc method:[28]

$$\alpha h\upsilon \propto (h\upsilon - E_g)^n$$

where υ is the frequency of the photon, *h* is the plank's constant, $E_g$ is the optical gap energy, α is the absorption coefficient and *n* equals 2 for indirect and ½ for direct allowed transitions respectively. The gap energy of $SnO_2$ ranges from 3.5 to 3.8 eV.[29,30] The gap energy of S, T and TS films were approximated to be 3.60, 3.17 and 3.71 eV respectively as indicated in Fig. 4. The slight increase in the composite gap energy can be traced to the relative positions of the conduction bands (CB) and valence bands (VB) of $SnO_2$ and $TiO_2$. The both CB and VB of SnO2 are slightly above that of $TiO_2$ with a difference of around 0.14 and 0.64 eV respectively [31]. When analyzing the films with UV-Vis, the interaction will be collective and we observe the overall gap to be from the VB of $TiO_2$ to the CB of $SnO_2$ which correlates perfectly with our results, that is a slight increase of the TS film (3.71 eV) compared to S film gap (3.60 eV).

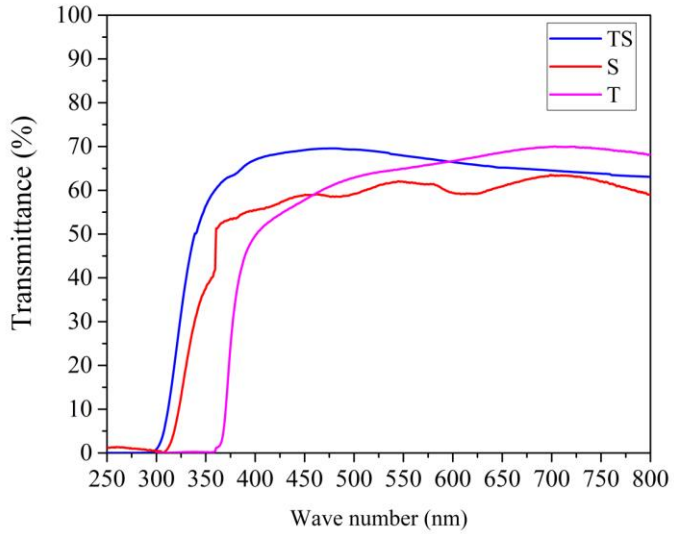


Fig. 3 – Transmittance spectra of TS, T and S films.

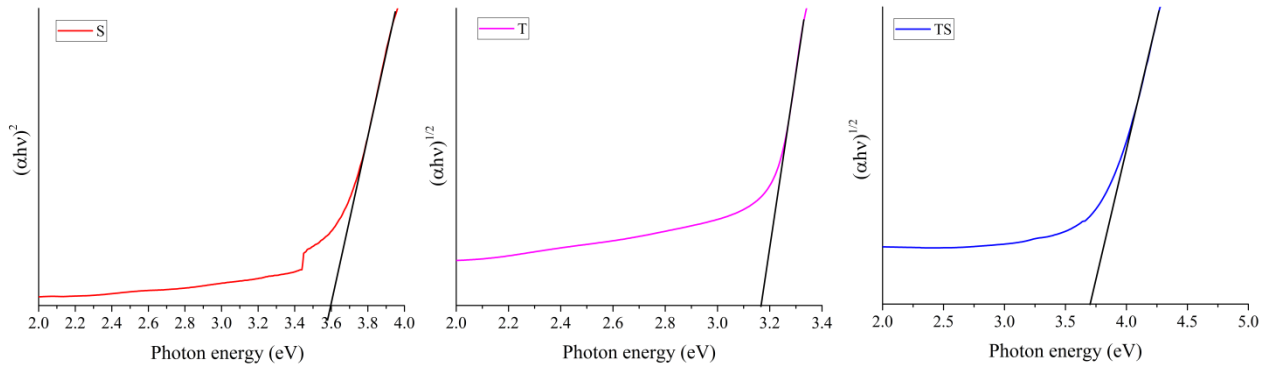


Fig. 4 – Tauc plot of the various films.

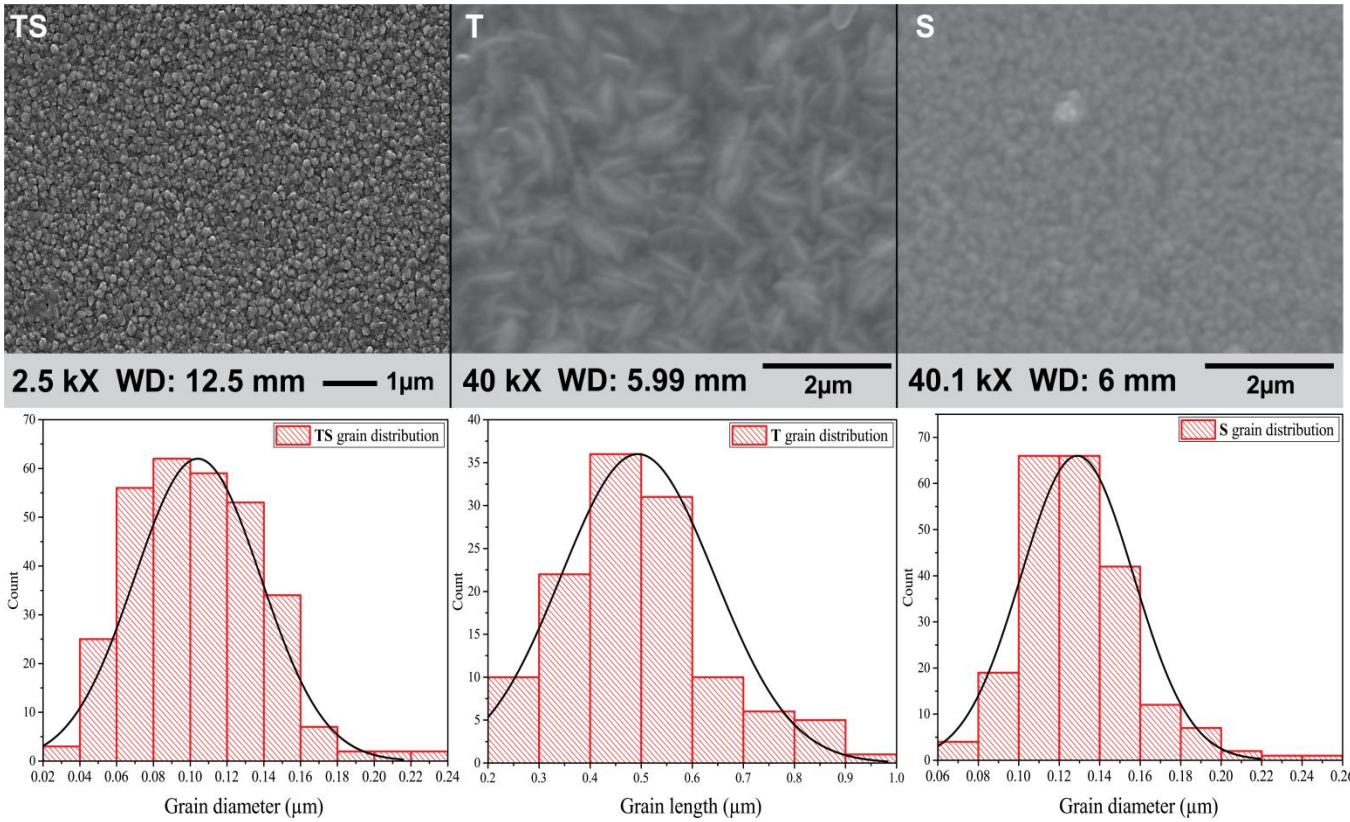


Fig. 5 – SEM Surface morphology images and histogram of the deposited films.

## 3. SEM images and surface morphology

The surface morphology of all the films (Fig. 5) seemed to have a homogenous grain distribution as clearly shown in the histogram where the normal distribution peak is narrow. The TS films had grain size ranging from 70 to 140 nm with almost spherical-like shape with an average size of 100 nm. The same grain shape can be observed for S film with grain size in the interval of 100 to 160 nm and average of 130 nm. The T film on the other hand had somewhat different morphology, where elongated grains are observed with an average length of 500 nm. From Figs. 2 and 5 we can see that the crystallite size and the grain size of the S film are almost the same but in the case of T and TS films the grain is comprised of smaller crystallites. The surface morphology relies on variety of physical entities and preparation conditions dealing with spray pyrolysis process. These parameters can be: the solution viscosity and precursor concentration.[32]

## 4. Photocatalytic activity

The photocatalytic performance of T, S and TS films was evaluated by degradation of sunset yellow dye under UV-light radiation. The temporal variation of the dye concentration by the catalyst effect of the films was monitored by the absorption peak at 482 nm and it is depicted in Fig. 6. After 18 hours, the degradation percentage of TS nanocomposite film reached 90.27%which is very superior to that of T and S films as they exhibited a maximum percentage of degradation of 29.65% and 19.74% respectively. The results are accordance with the literature where $SnO_2$-$TiO_2$ was found to exhibit an enhancement in photodegradation of acrylic acid.[33] For an insight on the kinetic of the reaction, the results were fitted to pseudo first order reaction.[34]

$$\frac{dC}{dT} = -kC$$

where $k$ is a reaction rate (positive constant) and $C$ is the concentration at time t, or equivalently using the percentage of degradation $X$.

$$\frac{dX}{dT} = k(1 - X)$$

The percentage of degradation then can be fitted by the following equation

$$X = A(1 - \exp(-kt))$$

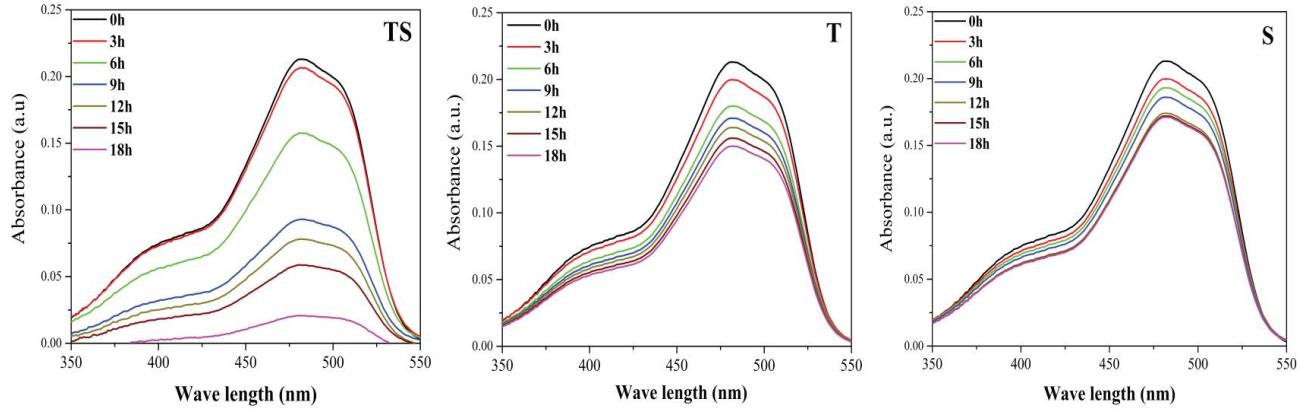


Fig. 6 – Sunset yellow dye degradation by the individual films.

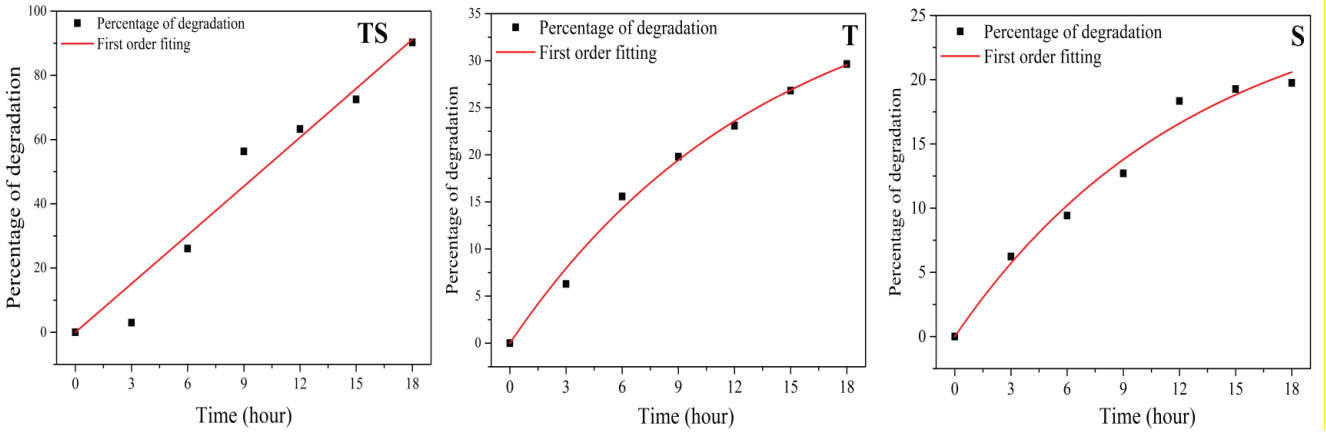


Fig. 7 – Percentage of degradation and first order chemical reaction fitting for all the films.

To quantify the fitness of the first order chemical reaction, the coefficient of determination (COD) was set as the criterion. COD is a number between 0 and 1. If it is 0, it indicates that the fit explains none of the variability of the response data around its mean, while if COD is 1; it indicates that the fit explains all the variability of the response data around its mean. In general, the larger the COD, the better the fit explains the data.[35] The fitting of the degradation percentage are depicted in Fig. 7. All of the films had COD above 0.95, which is an indication that the kinetics of the photocatalysis activity of the films was indeed a first order chemical reaction. $SnO_2$ does not perform well as photocatalysis, most likely due to the relative position of its conduction band, which is insufficient for reducing oxygen molecular to a superoxide anion.[36] The enhancement in the performance of the TS film relative to T and S films can be attributed to the formation of n–n heterojunction which plays an essential role in the effective separation of light induced electrons and holes. Both the $SnO_2$ and $TiO_2$ are identified as n-type semiconductors. The Conduction Band (CB) and the Valence Band (VB) positions of $TiO_2$ are more negative than $SnO_2$,[37] therefore, when band gap excitation occurs in $TiO_2/SnO_2$ n–n heterojunction, the electron-hole pairs in $TiO_2$ are generated first since its Fermi energy level is higher than that of $SnO_2$ due its smaller work function.[38] Afterwards, the electron migrates from CB of $TiO_2$ to that of $SnO_2$ and the hole migrates from VB of $SnO_2$ to that of $TiO_2$. The charge transfer between $TiO_2$ and $SnO_2$ effectively separates the electrons and holes pairs.[39] Dye degradation in $TiO_2$ is dominated by indirect mechanisms generally dominant rather than direct mechanism.[40–42] The indirect dye degradation mechanism relay on ionization of water at the semiconductor surface, where the photogenerated holes at the valence band react with water to produce $OH^{\cdot}$ radical, the later is highly oxidizing element. It reacts with adsorbed dye molecules or those very close to the catalyst surface.[43] An increase in the electron hole separation inside the semiconductor is therefore a direct increase in its efficiency.

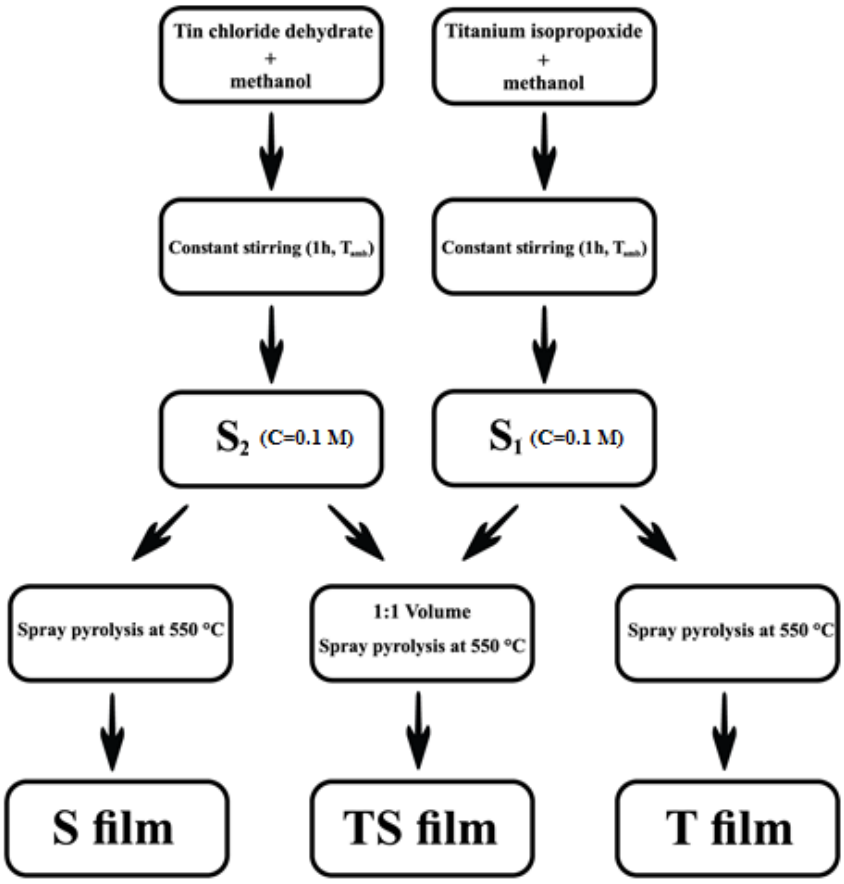


Fig. 8 – Solution preparation and deposition process.

## EXPERIMENTAL

In this work, spray pyrolysis deposition method was used to deposit the TiO2, SnO2 and their composite on ordinary glass substrates. For that, the sprayed solutions at 0.1 M in methanol were prepared at room temperature under constant stirring for one hour in open air. The first solution (S1) was prepared by dissolving titanium isopropoxide (C12H28O4Ti, Aldrich purity > 97%) in methanol. The second solution (S2) was prepared by dissolving tin chloride dehydrate (SnCl2 2H2O, Biochem purity > 98%) in methanol. The substrates were ultra-sonically cleaned in a 1:1 bath of acetone and methanol at T=40 °C for 10 minutes then dried in air. The T film was obtained by spraying the solution S1, S film was obtained by spraying S2 and TS film was obtained by spraying a mixture, (1:1) of S1 and S2. The total volume sprayed for each film was 10 mL at a rate of 1 mL/min. The distance nozzle-substrate was kept at 20 cm and the heating plate at 550 °C. To characterize the films, the X-Ray Diffraction (XRD) analyses was performed using ARL EQUINOX 100 X-ray diffractometer. To examine the surface morphology, a Tescan Vega 3 Scanning Electron Microscope (SEM) was employed. To assess their transmittance, the obtained films were scanned by UV-Visible light from 250 to 800 nm using JASCO V-630 spectrophotometer. For the photocatalysis assay, sunset yellow was used at a concentration of $5 \times 10^{-6}$M, pH of 8.8, under ambient temperature and a 280 nm UV lamp was used to activate the process. The absorbance was evaluated by the same UV-Vis spectrophotometer. The following diagram summaries the solution preparation and deposition.

## CONCLUSIONS

In summary, the synthesis of $SnO_2$ and $TiO_2$ and their composite $SnO_2$-$TiO_2$ films abbreviated as S, T and TS respectively is carried out. From XRD analysis, all of the films were polycrystalline and mixed phase. The S films exhibited $SnO_2$ and traces of SnO with the biggest crystallite size of 115 nm, where T and TS film had crystallite size of 21.5 and 18.8 nm respectively. All of the films experienced tensile strain. The UV-Vis measurement indicated a fairly high transmittance for T and TS films, the gap energy was calculated from the Tauc plot to be 3.60, 3.17 and 3.71 eV for S, T and TS respectively. The SEM images revealed homogenous grain distribution with different shapes (spherical like in S and TS and elongated for T). Finally the photocatalysis of sunset yellow dye by the three films was enhanced by the formation of n-n heterojuction in the TS film to reach 90.27%. All of the films photocatalysis behavior was really close to a first order chemical reaction. The elaborated films promise a cleaner, cheap and efficient way to reduce environmental hazards of sunset yellow dye

with the possibility of reusing them due to their thin films nature.

## REFERENCES


1. G. S. Shankarling, P. P. Deshmukh and A. R. Joglekar, *J. Environ. Chem. Eng.*, **2017**, *5*, 3302–3308. https,//doi.org/10.1016/j.jece.2017.05.057.
2. O. I. Lipskikh, E. I. Korotkova, Ye. P. Khristunova, J. Barek, and B. Kratochvil, *Electrochim. Acta*, **2018**, *260*, 974–985. https,//doi.org/10.1016/j.electacta.2017.12.027.
3. S. Benkhaya, B. Achiou, , M. Ouammou, , J. Bennazha, , S. Alami Younssi, S. M'rabet and A. El Harfi, *Mater. Today Commun*, **2019**, *19*, 212–219. https,//doi.org/10.1016/j.mtcomm.2019.02.002.
4. L. F. Cusioli, H. B. Quesada, A. T. A. Baptista, R. G. Gomes and R. Bergamasco, *Environ. Prog. Sustain. Energy*, **2020**, *39*, e13328. https,//doi.org/ 10.1002/ep.13328.
5. D. Rajamanickam and M. Shanthi, *Spectrochim. Acta Part A: Molec. and Biomolec. Spectroscopy*, **2014**, *128*, 100–108. https,//doi.org/10.1016/j.saa.2014.02.126.
6. M.-L. Kääriäinen, T. O. Kääriäinen and D. C. Cameron, *Thin Solid Films*, **2009**, *517*, 6666–6670. https//doi.org/ 10.1016/j.tsf.2009.05.001.
7. M. Kitano, K. Tsujimaru and M. Anpo, *Appl. Catal A: General*, **2006**, *314*, 179–183. https,//doi.org/10.1016/j.apcata.2006.08.017.
8. B. Pant, M. Park and S. J. Park, *Coatings*, **2019**, *9*, 613. https,//doi.org/10.3390/coatings9100613.
9. P. Phuinthiang, D. T. T. Trinh, D. Channei, K. Ratananikom, S. Sirilak, W. Khanitchaidecha and A. Nakaruk, *J. Nanomater.*, **2021**, *11*, 1493. https,//doi.org/ 10.3390/nano11061493.
10. C. Wu, Q. X. Wu and W. Y. Chen, *Adv. Mat. Res.*, **2011**, *347-353*, 137–141. https//doi.org/10.4028/ www.scientific.net/amr.347-353.137.
11. J. M. Rzaij and M. A. Abass, *Chem. Rev.*, **2020**, *2*, 114–121. https,//doi.org/10.33945/sami/jcr.2020.2.4
12. H. Peeters, M. Keulemans, G. Nuyts, F. Vanmeert, C. Li, M. Minjauw, C. Detavernier, S. Bals, S. Lenaerts and S. W. Verbruggen, *Appl. Catal. B: Environ.*, **2020**, *267*, 118654. https,//doi.org/10.1016/j.apcatb.2020.118654.
13. K. Tanaka, M. F. V. Capule and T. Hisanaga, *Chem. Phys. Lett.*, **1991**, *187*, 73–76. https,//doi.org/10.1016/ 0009-2614(91)90486-s.
14. C. H. Kwon, J. H. Kim, I. S. Jung, H. Shin and K. H. Yoon, *Ceram. Int.*, **2003**, *29*, 851–856. https,//doi.org/ 10.1016/s0272-8842(03)00019-1.
15. C. M. Firdaus, M. S. B. Shah. Rizam, M. Rusop and S. Rahmatul. Hidayah, *Procedia Eng.*, **2012**, *41*, 1367–1373. https,//doi.org/10.1016/j.proeng.2012.07.323.
16. Sk. T. Ahamed, A. Ghosh, B. Show and A. Mondal, *J. Mater. Sci. Mater*, **2020**, *31*, 6616-16633. https,//doi.org/10.1007/s10854-020-04217-6.
17. S. Balamurugan and A. R. Balu, *J. Electron. Mater*, **2019**, *19*, 212–219. https,//doi.org/10.1016/ j.mtcomm.2019.02.002.
18. N. Abdullah, N. M. Ismail and D. M. Nuruzzaman, *Mater. Sci. Eng.*, **2018**, *319*, 012022. https,//doi.org/ 10.1088/1757-899x/319/1/012022.
19. A. Fuchs, H.-J. Schimper, A. Klein and W. Jaegermann, *Energy Procedia*, **2011**, *10*, 149–154. https,//doi.org/ 10.1016/j.egypro.2011.10.168.
20. T. Shukla, *J. Sens. Sci. Technol.*, **2012**, *02*, 102–108. https,//doi.org/10.4236/jst.2012.23015doi: 10.4236/ jst.2012.23015.
21. Y. Li, W. Yin, R. Deng, R. Chen, J. Chen, Q. Yan, B. Yao, H. Sun, S.-H. Wei and T. Wu, *NPG Asia Mater.*, **2012**, *4*, e30–e30. https,//doi.org/10.1038/am.2012.56.
22. S. Das and V. Jayaraman, *ChemInform*, **2014**, *66*, 112–255. https,//doi.org/10.1016/j.pmatsci.2014.06.003.
23. S. Senthil, S. Srinivasan, T. Thangeeswari, B. J. Madhu and M. Silambarasan, *Nano-Struct. Nano-Objects*, **2020**, *24*, 100554. https,//doi.org/10.1016/j.nanoso.2020.100554.
24. A. A. Ambalkar, R. P. Panmand, U. V. Kawade, Y. A. Sethi, S. D. Naik, M. V. Kulkarni, P. V. Adhyapak and B. B. Kale, *New J. Chem.*, **2020**, *44*, 3366–3374. https,//doi.org/10.1039/c9nj06110j.
25. T. Isono T. Fukuda, K. Nakagawa, R. Usui, R. Satoh, E. Morinaga and Y. Mihara, *SID Symposium Digest of Technical Papers*, **2006**, *37*, 1874. https,//doi.org/ 10.1889/1.2433411.
26. D. Nath, F. Singh and R. Das, *Mater. Chem. Phys.*, **2020**, *239*, 122021, doi: 10.1016/j.matchemphys.2019.122021.
27. Z. S. Khalifa, *RSC Adv.*, **2017**, *7*, 30295–30302. https,//doi.org/10.1039/c7ra00706j.
28. B. Bharti, S. Kumar, H.-N. Lee and R. Kumar, *Sci. Rep.*, **2016**, *6*, 32355. https,//doi.org/10.1038/srep32355.
29. S.-L. Chen, A.-J. Wang, C. Dai, J. B. Benziger and X.-C. Liu, *Chem. Eng. J.*, **2015**, *10*, 200. https,//doi.org/ 10.1186/s11671-015-0901-8.
30. Y. Chen, B. Liu, J. Chen, L. Tian, L. Huang, M. Tu and S. Tan, *Nanoscale Research Letters*, **2015**, *10*, 200. https,//doi.org/10.1186/s11671-015-0901-8.
31. D. Talinungsang, D. D. Upadhaya, D. D. Purkayastha and M. G. Krishna, *Mater. Chem. Phys.*, **2020**, *241*, 122333, doi: 10.1016/j.matchemphys.2019.122333.
32. O. J. Ilegbusi, S. M. N. Khatami and L. I. Trakhtenberg, *Mater. Sci. Appl.*, **2017**, *08*, 153–169. https,//doi.org/ 10.4236/msa.2017.82010.
33. J. Zhang, L. Feng, J. Wei, X. Guo and W. Cao, *Chin. Sci. Bull.*, **2006**, *51*, 2050–2054. https,//doi.org/10.1007/ s11434-006-2083-3.
34. C. Ampelli, D. Di Bella, D. G. Lister and G. Maschio, *J. Therm. Anal. Calorim.*, **2005**, *79*, 89–94. https,//doi.org/10.1007/s10973-004-0567-4.
35. L. D. Schroeder, D. L. Sjoquist and P. E. Stephan, "Understanding regression analysis: an introductory guide", Los Angeles, London, New Delhi: Sage, 2017.
36. M. Grätzel, *Nature*, **2001**, *414*, 338–344, doi: 10.1038/35104607.
37. M. Zhou, J. Yu, S. Liu, P. Zhai and L. Jiang, *J. Hazard. Mater.*, **2008** *154*, 1141–1148. https,//doi.org/10.1016/ j.jhazmat.2007.11.021.
38. C. Wang, C. Shao, X. Zhang and Y. Liu, *Inorg*, **2009**, *48*, 7261–7268. https://doi.org/10.1021/ic9005983
39. D. Talinungsang, D. Upadhaya, D. Purkayastha and M. G. Krishna, *Mater. Chem. Phys.*, **2020**, *241*, 122333. https,//doi.org/10.1016/j.matchemphys.2019.122333.
40. C. Galindo, P. Jacques and A. Kalt, *J. Photochem. Photobiol. A*, **2000**, *130*, 35–47, https://doi.org/10.1016/ S1010-6030(99)00199-9.
41. Y. Ma and J.-n. Yao, *J. Photochem. Photobiol., A*, **1998**, *116*, 167–170, https://doi.org/10.1016/S1010-6030(98)00295-0.
42. F. Chen, Y. Xie, J. Zhao and G. Lu, *Chemosphere*, **2001**, *44*, 1159–1168, https://doi.org/10.1016/S0045-6535(00)00277-0.
43. J. Saien and A. R. Soleymani, *J. Ind. Eng. Chem.*, **2012**, *18*, 1683–1688, https://doi.org/10.1016/ j.jiec.2012.03.014.